Equidimensional Fractal Maps for Indirect Estimation of Deformation Damage in Nonuniform Aircraft Alloys

E.E. Zasimchuk, Yu.G. Gordienko, R.G. Gontareva, and I.K. Zasimchuk

(Submitted 29 May 2001)

This article describes the surface relief formation on Al single-crystal plates (sensors) with orientation {100}<001> that were rigidly attached to weld specimens of aircraft alloy 2024 T351 during fatigue loading. Taking into account the nonuniform structure of the weld alloy, we located sensors in different zones of the weld specimens to receive information about the sites of strain localization and probability of destruction. The qualitative and quantitative information about the sensor relief was extracted by the online method automated on the basis of a stereomicroscope with a charge-coupled device (CCD) camera attached to a personal computer by a video adapter and frame-grabber card. The quantitative and qualitative relief parameters are shown to correlate with the deformation prehistory of the weld specimens. Panoramic views were created and used for fractal analysis of deformation relief. Spatial distributions of information fractal dimension on the sensor surface for different numbers of cycles were plotted in the shape of contour lines with equal values (equidimensional maps). Equidimensional maps for sufficiently large sensors allow us to find strain localization sites in specimens and monitor their evolution in an online regimen.

Keywords damage, diagnostics, fatigue, fractal, weld

1. Introduction

In our previous works,[1-3] we investigated the surface relief of single-crystal aluminum foils with orientation <221>{110}, which were rigidly attached to specimens of complex aircraft alloy during fatigue loading of the alloy. The density and direction of relief bands were shown to correlate with the number of loading cycles at early stages of loading. We proposed to use such single-crystal foils as the sensors of fatigue damage.

To date, we have investigated only one orientation of single-crystal foils and only two amplitudes of applied stresses: 140 and 180 MPa.[1-3] Therefore, our results were quite limited and nonoptimal for practical usage. To improve the method, the relief analysis was automated by using a microscope with a video camera attached to a personal computer having special software for information monitoring. We investigated behavior of sensors with different crystallographic orientations under fatigue loading and concluded that the most informative orientation of Al single-crystal sensor is <100>{001}.[4] In such sensors a noncrystallographic deformation relief forms and undergoes significant changes during loading. Sensors with this orientation are suitable for forecasting deformation damage in aircraft alloys. However, surface relief on these sensors is very irregular. The band density counting we used earlier was proven to be inappropriate for characterization of such complex surface relief.[1-3] For this purpose, we need to apply more sophisticated mathematic and geometric approaches that can yield more accurate scientific output.

E.E. Zasimchuk, Yu.G. Gordienko, R.G. Gontareva, and **I.K. Zasimchuk,** G.V. Kurdyumov Institute for Metal Physics of the National Academy of Sciences of Ukraine, 36 Vernadsky Blvd., 03142 Kiev, Ukraine. Contact e-mail: gord@imp.kiev.ua.

For specimens without weld zones and with unknown strain localization sites, we used methods of fractal analysis that are applicable for objects with self-similarity on different scale levels.[4] We calculated the information fractal dimension D of panoramic views of surface relief. From dependencies of D on the number of cycles for some stress amplitudes, one can derive conclusions about the current deformation prehistory. For example, when sites of strain localization in a parent material are absent, we proposed the following criterion of basic material lifetime: The maximal fractal dimension can be a sign of minimally permissible lifetime for the given deformation conditions and the material used.[4] The quantitative method of calculation of D presumes calculation of its average value for the whole surface of the sensor. This procedure is assumed to be meaningful for specimens without macroscopic stress concentrator sites. This condition, however, is not fulfilled for weld specimens with heterogeneous soft zones near the weld. This article proposes a new method of indirect estimation of heterogeneous deformation damage by means of quantitative fractal analysis of sensor surface relief on the basis of calculation of equidimensional fractal maps.

2. Experimental

2.1 Sensor and Specimen Preparation

We used the friction stir welding (FSW) process for welding plates of alloy 2024 T351 with a thickness 6.35 mm. The specimens with welded joints were cut from these plates. Microhardness analysis and x-ray methods were applied for investigation of different zones near the weld. In addition, sensors were glued over these zones on three sides of the specimen (see Section 3.1). By means of a special electric erosive device, they were cut from high-purity aluminum single crystals (99.995 wt.% Al). Cylindrical single crystals with a diameter of 15 mm were grown by the vertical Bridgeman method from seeds with the required axial orientation in an yttrium oxide

crucible. After the plates were cut, they were 0.3-0.5 mm thick, 30 mm long, 10 mm wide, and an orientation of {100}<100>. Orientations for cutting were verified by means of an x-ray diffractometer with the special portable crystal holder, which can be used with an x-ray goniometer, and then in a cutting machine. Cutting was performed by a 100-μm-wide brass wire with water-cooling under relatively moderate conditions: voltage $U = 600$ V, current strength $I = 70$ mA, and frequency $f = 22$ Hz.

Plates were initially polished from one facial side by the thin (micrometer scale) abrasive material for removal of stairs created by cutting. Plates then were electrically polished down to a width of 0.2 mm and a glassy smooth surface was obtained. This process removed the external layer of single-crystal plates that was damaged significantly by electric discharges during electric erosive cutting. However, after final polishing, the single-crystal plates contained (as observed by x-ray topography[5]) the characteristic regular defect structure, which caused strengthening of plates in comparison to the initial single crystal. Such a structure can be obtained either by chemical cutting or by electric erosive polishing (near to 1 mm on each side). We did not, however, discover the influence of a regular defect structure in single-crystal plates on the deformation process and evolution of deformation substructure. Therefore, we used the plates with a faintly pronounced initial defect structure. Sensors were classified according to their location in the zones: small sensors (from 5 × 5 to 10 × 10 mm) for all zones and large sensors for a narrow weld side (with narrow weld zone) (~10 × 20 mm). Sensors were fixed by means of PASCOFix glue (Pasco-Handels GmbH, Berlin, Germany) on flat surfaces of the specimens for additional mechanical testing.[4] Loading of specimens with sensors was carried out on a hydropulse machine with working frequency ~11 Hz at room temperature. The range of applied stresses was equal to 140-240 MPa, at which a specimen always was deformed in an elastic regimen, and the sensor was deformed in plastic. The shape of the loading cycle was saw-like, with minimal loading value near zero. (The mechanical testing was performed at Kiev University of Civil Aviation by M.V. Karuskevich.)

2.2 Image Acquisition

The qualitative and quantitative information about a deformation relief was extracted by the automated method using a stereomicroscope (model GZ7, Leica Inc., Buffalo, NY) with a charge-coupled device (CCD) camera (model XC-77, Sony, USA) attached to a personal computer (Pentium II class) by video adapter and frame-grabber card (Oculus TCi Ultra II, Coreco Inc., St-Laurent, Quebec, Canada). For sensor surface characterization, panoramic views of sensor surfaces were created automatically by means of the specially designed software and fractal analysis was applied for image data processing. Two types of illumination were used: directional and diffuse ring illumination. At certain breakpoints of loading, the specimens were scanned by the microscope and many single snapshots of a sensor surface were created. To acquire the whole set

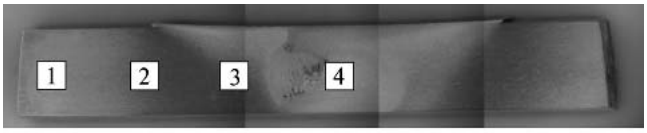

(a)

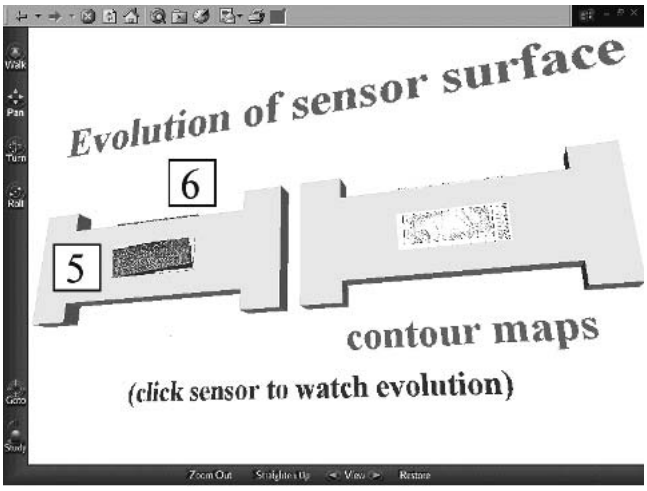

(b)

Fig. 1 **(a)** The macrostructure of long flank side of welded plate (1, parent metal; 2, TMAZ; 3, weld/TMAZ transition zone; 4, weld) and screen-shot of the virtual model with schematic view on sensor locations, and **(b)** dynamic representation of the tests results (5, narrow weld side; 6, flank side)

Table 1 Half-Widths (B) of Diffraction Lines (400) and (422) in Separate Zones of a Welded Joint

	$B \times 10^2$, radian	
Zone	**Line (400)**	**Line (422)**
Parent metal	1.395	1.549
TMAZ	1.462	1.583
Weld/TMAZ transition zone	1.201	1.409
Weld	1.148	1.375

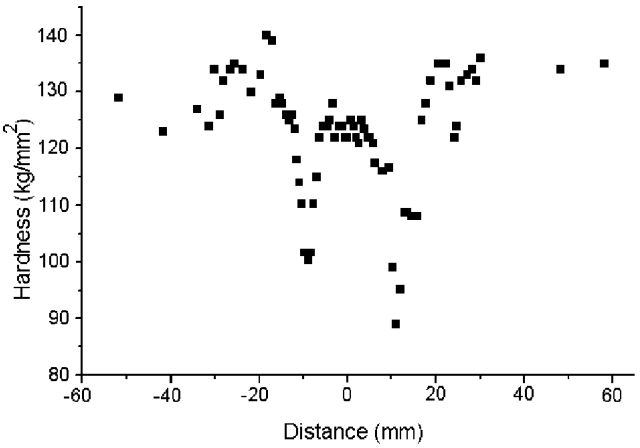

Fig. 2 Hardness profile along the welded joint on the wide weld side

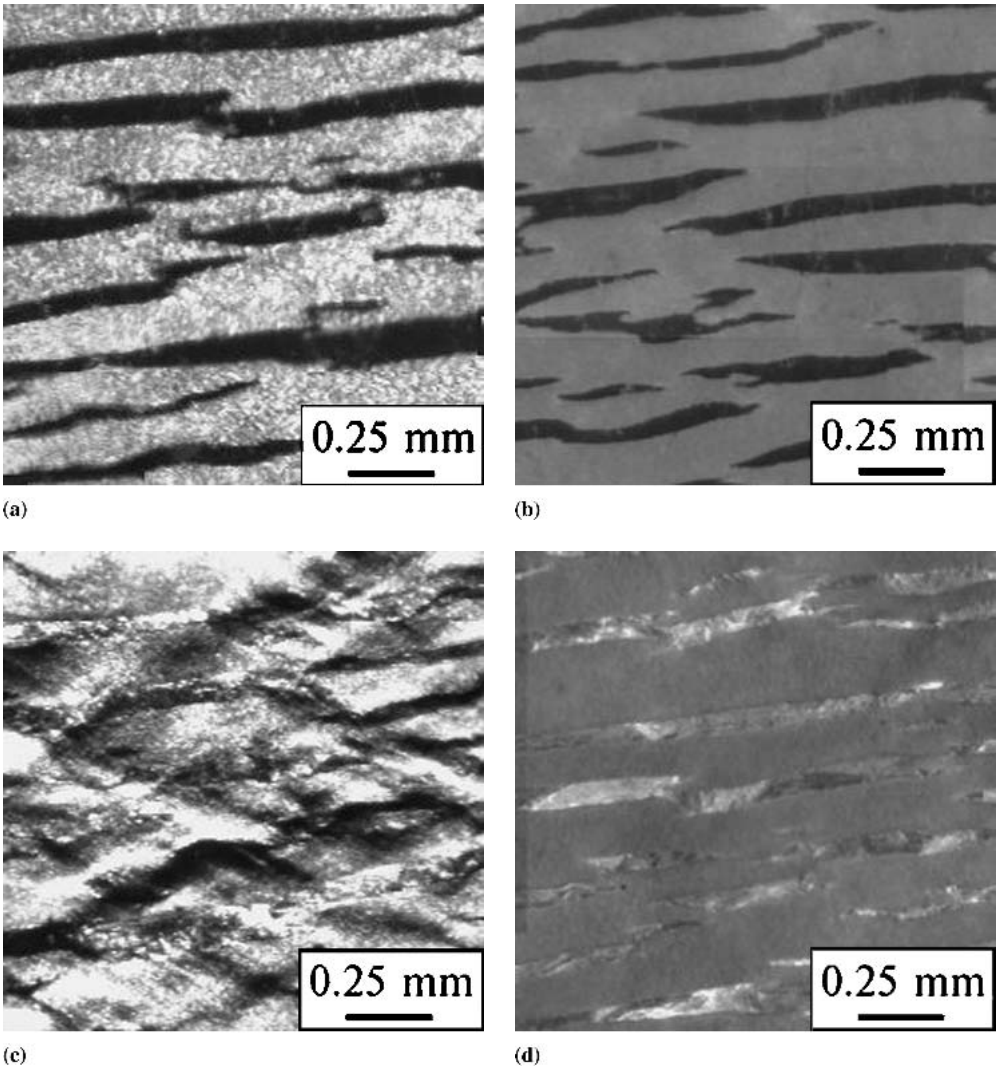

Fig. 3 Typical images of sensor surface under different illumination: **(a)** and **(b)** initial stages (24 000 cycles); **(c)** and **(d)** late stages (800 000 cycles); (a) and (c) directed illumination; (b) and (d) diffuse ring illumination (175 MPa)

of snapshots for diffuse ring illumination (directed illumination), we used 200-300 (100-200 directed illumination) iterations of precise shifting and manual focusing at each image capturing point (Fig 3). The minimal average overlapping of snapshots of neighboring regions was 15%, but for better performance on the next stage (panoramic view creation), overlapping of snapshots up to 30% was used.

Panoramic view creation was fulfilled by means of specially prepared software for automatic merging of panoramic photos (with appropriate adjustment) and manual debugging of erroneously located snapshots. The main problems were related to inadequate software used for this purpose. The software was initially designed for merging natural scene images with a full-color (32-bit) palette and often led to erroneous results for specific (band-like[4,6]) images with a 256-color (8-bit) palette. The additional errors appeared because of the self-similar nature of band-like patterns on a sensor surface. In future work, new software will be elaborated to produce better quality panoramas.

2.3 Multiscale Data Processing

Data processing of panoramic images was carried out on the basis of the algorithms described below. For application of fractal analysis, one must find the scope of self-similarity for the property investigated. This task is highly dependent on physical sizes of the system, because mathematical definition of self-similarity in relation to physical objects is greatly concerned with certain size limitations. We used three measures along the *x*-axis (along tension direction), *y*-axis (perpendicular to tension direction), and the so-called *z*-axis (coloration values). The lowest scale level for digitized images is theoretically limited by the lowest value optical resolution of the Sony XC-77 CCD camera. In the case described in this article, it was equal to one pixel. Taking into account the precautions of the manufacturer, we used an optical resolution of 2-3 pixels. The highest scale level in the *x*-*y* plane was theoretically limited by the size of digitized image, which was equal to 480 × 640 pixels for a single image and ~5000 × 10 000 pixels for pan-

oramic view. In this work, all images were captured in gray scales from 0 (black) to 255 (white); that is why the highest scale level in the z-axis was limited to 256 levels, and the appropriate three-dimensional (3D) basin of investigation was limited by the lowest range by z-axis and was equal to 256 × 256 × 256 (i.e., slightly more than two decades).

Note that for quantitative characterization, one needs the knowledge of the true 3D-representation of the whole sensor surface relief. In this case, some projections of this 3D-representation created by directed and diffuse ring illumination were used. These projections are only manifested in different coloration (z-axis). The main idea is supported by theoretical conjectures that projections of self-similar objects inherit the self-similarity of original objects.[7] Under these conditions, we considered two types of the processed patterns:

- irregular coloration pattern in 3D-embedding space; i.e., the gray-scale map with the spatial x-axis, the spatial y-axis, and coloration z-axis; and
- irregular coloration pattern in two-dimensional (2D) embedding space; i.e., the gray-scale map with the spatial x-axis (or y-axis) and coloration z-axis.

The core formula that was used for calculation of information fractal dimension (D) for the sample set covered by the number $N(e)$ of cells of size e with probability $P(e,i)$ that a point of the sample set is in ith cell is as follows:

$$D = \lim_{e \to 0} \left(\frac{\log [I(e)]}{\log [1/e]} \right)$$

where

$$I(e) = \sum_{i=1}^{N(e)} - P(e,i) \log [P(e,i)]$$

and $I(e)$ is the average surprise in learning which e-cell a point is in. For example, the maximum value of $I(e)$ can be reached for equal $P(e,i)$ for the given e (i.e., for the homogeneous distribution of points). The lower values of $I(e)$ can be interpreted as a measure of nonuniformity of the distribution of points. We preferred to use the information dimension because it gives the richest and most useful information. We carried out some tests on the objects with the well-known fractal dimension and the information dimension was the most adequate method among other box-counting methods. On the basis of the general idea of calculation and core formula,[8] we developed the code and used it for additional calculations.

3. Results and Discussion

3.1 Macrostructure of Welded Plates, Hardness, and Microscopic Distortions of Crystalline Lattice in Different Zones

The macrostructure of the long flank side of a welded plate is shown in Fig. 1(a). From these optical data, one can easily see the weld joint in the shape of trapezoidal light contrast. On the basis of microstructure data, we estimated that the width of the weld zone is ~21 mm on the wide weld side (top of Fig. 1) and ~12 mm on the reverse narrow side (bottom of Fig. 1). Four different zones can be noted near the weld: 1, parent metal; 2, thermomechanically affected zone (TMAZ); 3, weld/TMAZ transition zone; and 4, weld. The schematic views of sensor locations near the weld at facial and flank sides are shown in Fig. 1(b), which is the screen-shot of the virtual model with schematic view of sensor locations and dynamic representation of the tests results.[6] Figure 2 illustrates the distribution of hardness along the welded joint on the wide weld side. The hardness value is nearly equal for the ranges more than 10 mm from the weld. Hardness changes along the longest side of the welded plate in a complicated manner. These changes correlate with the macrostructure of a welded joint (Fig. 1). The maximum hardness value is in a parent metal; in a weld, it is slightly higher than in surrounding regions, but lower than in a parent metal. TMAZs are located between the softest weld/TMAZ transition zone and parent metal. In these zones, hardness grows steadily from the minimum in the soft zone to the maximum in a parent metal.

Such heterogeneity of structure and properties is caused by complex phase and chemical composition of aircraft aluminum alloy 2024 T351. This alloy contains approximately 4.6% Cu, 1.5% Mg, 0.7% Mn, 0.4% Ti, and the balance Al. Solubility of all of these elements in aluminum is not very high at low temperatures (≤100 °C): Cu ~0.1%, Mg ~1.9%, Mn <0.3%, and Ti<0.07%.[9] However, solubility may be higher at higher temperatures and in the presence of a deformation process.

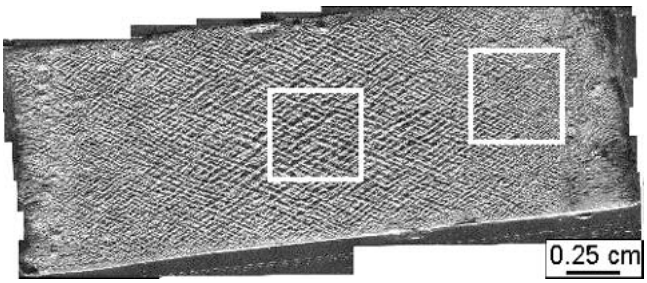

Fig. 4 Example of selection of ROI frame on image made from sensor surface (after 664 000 cycles, 232 MPa, directed illumination)

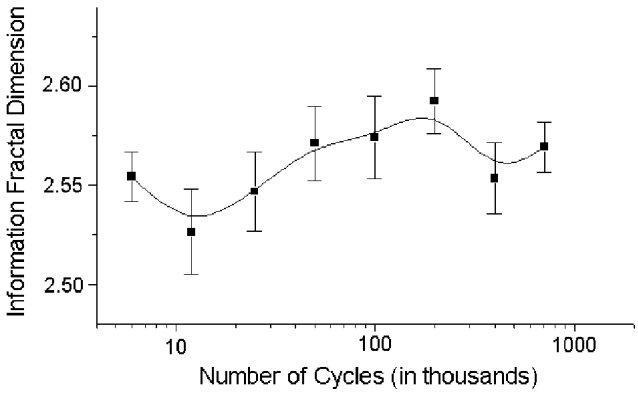

Fig. 5 Example of information dimension evolution averaged by ROI and the number of specimens (three items) in a parent metal

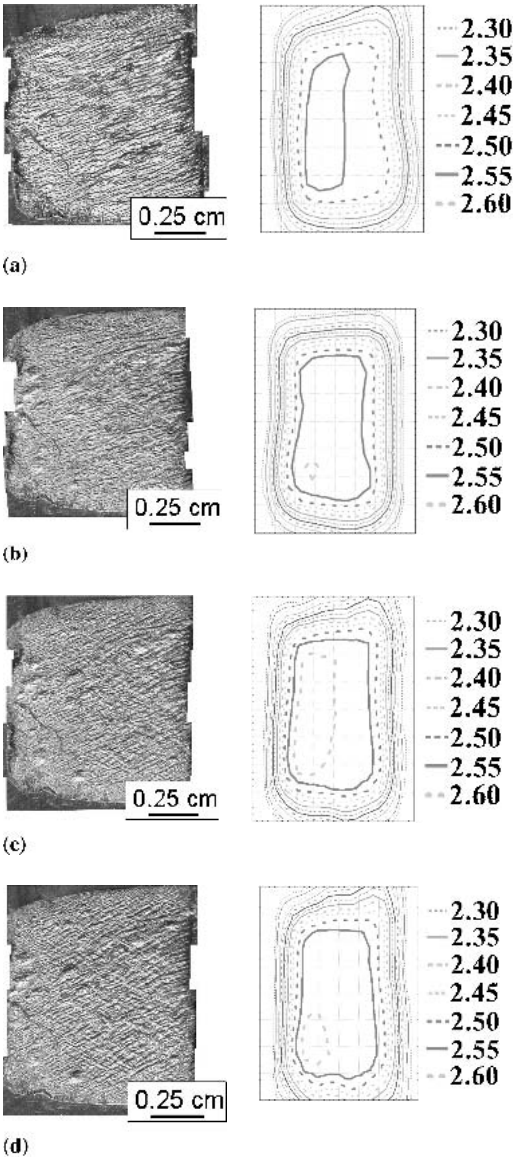

Fig. 6 Evolution of sensor surface (parent metal) visualized by panoramas (left column) and contour plots of information dimension (right column): **(a)** 25 000, **(b)** 100 000, **(c)** 200 000, and **(d)** 710 000

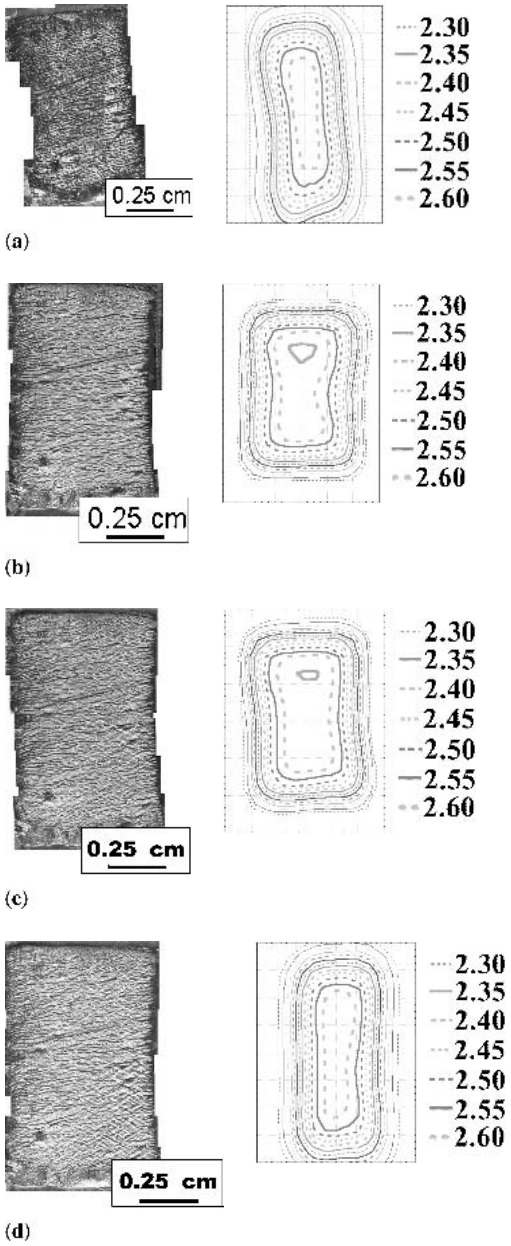

Fig. 7 Evolution of sensor surface (TMAZ) visualized by panoramas (left column) and contour plots of information dimension (right column): **(a)** 6000, **(b)** 50 000, **(c)** 100 000, and **(d)** 400 000

Therefore, many different inclusions can exist in a parent zone of alloy 2024 T351. Welding treatment can transform the phase composition of the alloy and decrease the quantity and size of inclusions. These changes can influence the properties of the alloy (Fig. 2). The quantity and size of second-phase particles can obviously affect microscopic distortions of crystalline lattice of the solid solution. For example, enlargement of particles can be accompanied by depletion of the solid solution and decrease in hardness. At the same time, the decrease of the number of particles is connected with enrichment of the solid solution and accompanied by an increase in hardness.

X-ray methods are known to be useful for analysis of the stressed state of a crystalline lattice independent of the appearance of this state. The stressed state of crystalline lattice stimulates x-ray diffraction (XRD) line broadening, and half widths of these lines can characterize the stressed state of crystalline material.[10] We examined half widths (B) of lines (400) and (422) on diffraction pictures of solid solution by XRD with simple harmonic Cu illumination. The values of half-width of x-ray lines (400) and (422) for a solid solution in a welded plate of alloy 2024-T351 are shown in Table 1.

The half-width of x-ray line (400) of pure aluminum is equal to ~0.5545×10^{-2} radian, which is essentially smaller than for a solid solution in all zones of the welded metal. If the deformation processes were inessential, the microscopic distortions would be dependent on the internal stresses caused by supersaturation or initial stages of dissociation of the solid

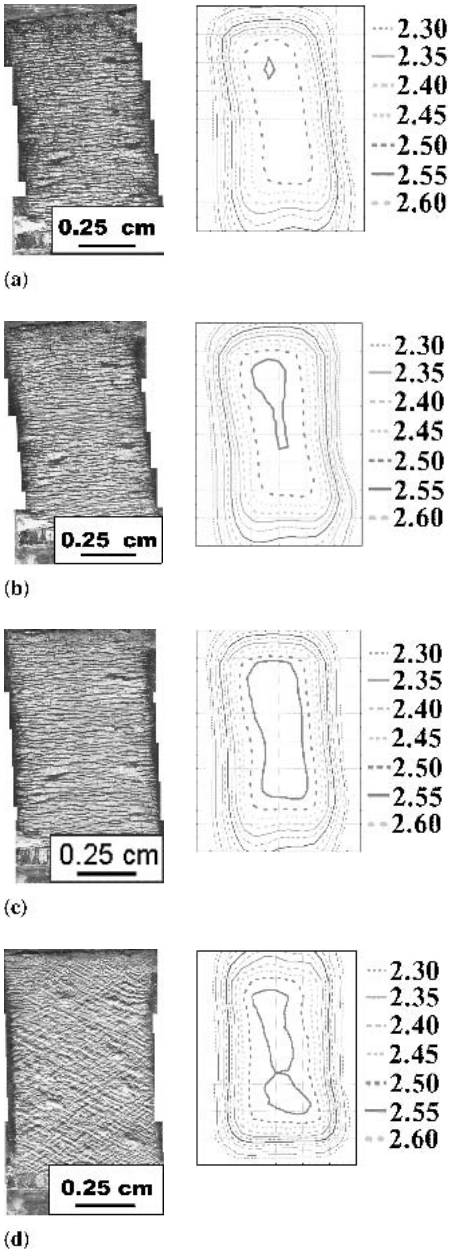

Fig. 8 Evolution of sensor surface (TMAZ/weld transition zone) visualized by panoramas (left column) and contour plots of information dimension (right column): **(a)** 6000, **(b)** 12 000, **(c)** 25 000, and **(d)** 400 000

solution. Coagulation of particles of the second phase leads to decrease of the crystalline lattice distortions. These processes can go off simultaneously during the weld procedure. Therefore, microscopic distortions in welded plates can have a very complex character. In our opinion, the low decrease of B in weld and weld/TMAZ transition zones (in comparison with a parent metal) is caused by several simultaneous processes: solid-solution break-up, coagulation of particles of the second phase, and repetitive dissolving of separations.

The hardness values (Fig. 2) are larger in a weld and therefore we can assume that dissolving of particles of the second

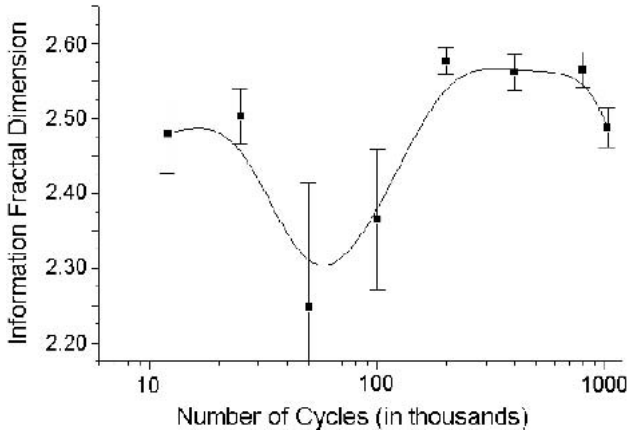

Fig. 9 Evolution of information dimension for sensor in a weld zone

phase (for example, the particles containing Mg) seems to be the leading process in a weld. However, an increase of temperature also can stimulate the coagulation of other separations and cause a decrease of B. In a weld/TMAZ transition zone, an increase of temperature is apparently not so large (in comparison with a weld). The small value of B and the minimum of hardness are probably caused by coagulation of different separations existing in alloy 2024-T351. The maximal value of B was observed in a TMAZ zone. This result is assumed to be connected with the presence of a large quantity of very small particles. These particles are picked out from a supersaturated solid solution because of the increase of temperature. It is not sufficient for coagulation of these separations, however, because it took place in a weld and weld/TMAZ transition zones. Our discussion of phase transformations in a welded plate of alloy 2024-T351 and their influence on properties of the alloy has only qualitative character. Nevertheless, the data obtained during our investigation allow us to imagine a priori the most probable map of strain localization sites. It can be very useful for determination of the places where sensors would be located.

3.2 Macrostructure of Sensor Relief

We scanned and processed all sensors under directed and diffuse ring illumination. Under directed illumination, we can qualitatively characterize evolution by the appearance of crossing systems of erections in two directions, and at the same time under diffuse ring illumination we can qualitatively characterize evolution by the splitting of initially black bands in many bright and dark small regions. These features may be classified (as bands, hills, ridges, blisters, etc.) and used for forecasting of a specimen's lifetime under loading.[11]

As discussed, we worked with sensors of different sizes and found some essential peculiarities. First, we noted that relief on small sensors in different zones does not differ significantly for the same stress level and the same number of cycles. In contrast, different parts of large sensors in the same zones can significantly differ. We assume that boundary effects can cause absence of difference in small sensors where areas of boundary regions cover a significant part of the whole sensor area. We suppose that all crystalline defects that take part in relief cre-

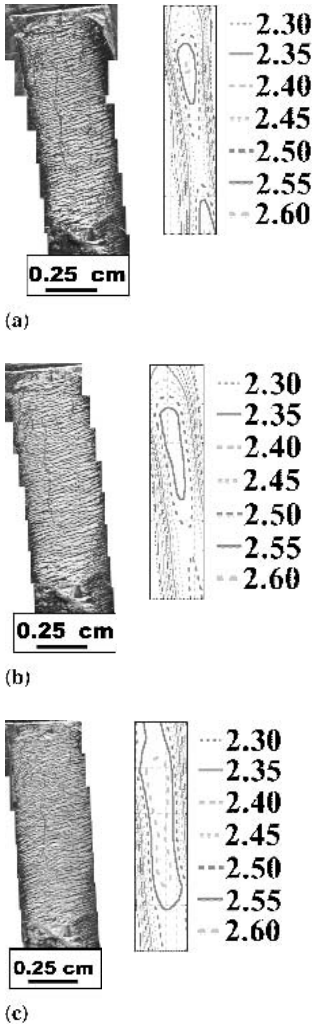

Fig. 10 Evolution of sensor surface (in a weld zone) visualized by panoramas (left column) and contour plots of information dimension (right column): **(a)** 12 000, **(b)** 25 000, and **(c)** 200 000 cycles.

ation can intensively sink in small sensors, but in large sensors these defects can be accumulated in central parts of sensors and lead to coarsening of the sensor relief.

3.3 Fractal Dimension of a Sensor Relief in Different Zones

For investigation of local properties of a sensor relief, we used the technique of moving region of investigation (ROI), (Fig. 4). An ROI frame with sizes 256 × 256 pixels was moved along the whole sensor surface (5000 × 2000 pixels) with a certain *x*-step and *y*-step (from 64-256 pixels). We calculated values of information dimension in 3*D* embedding space at each step and processed them. As a result, we visualized the distribution of information dimension on a sensor surface in the shape of contour lines with equal values and obtained the so-called contour equidimensional map.

3.3.1 Parent Metal. This zone is characterized by the highest hardness value in comparison to the other zones under investigation. Comparing it with our previous results, we achieved some correlation.[4] The evolution of information dimension averaged by area of ROI was nearly the same as it was in our previous tests with Al aircraft alloy specimens without stress concentrators.[4] The typical example of information dimension evolution for stress level 201 MPa is shown in Fig. 5.

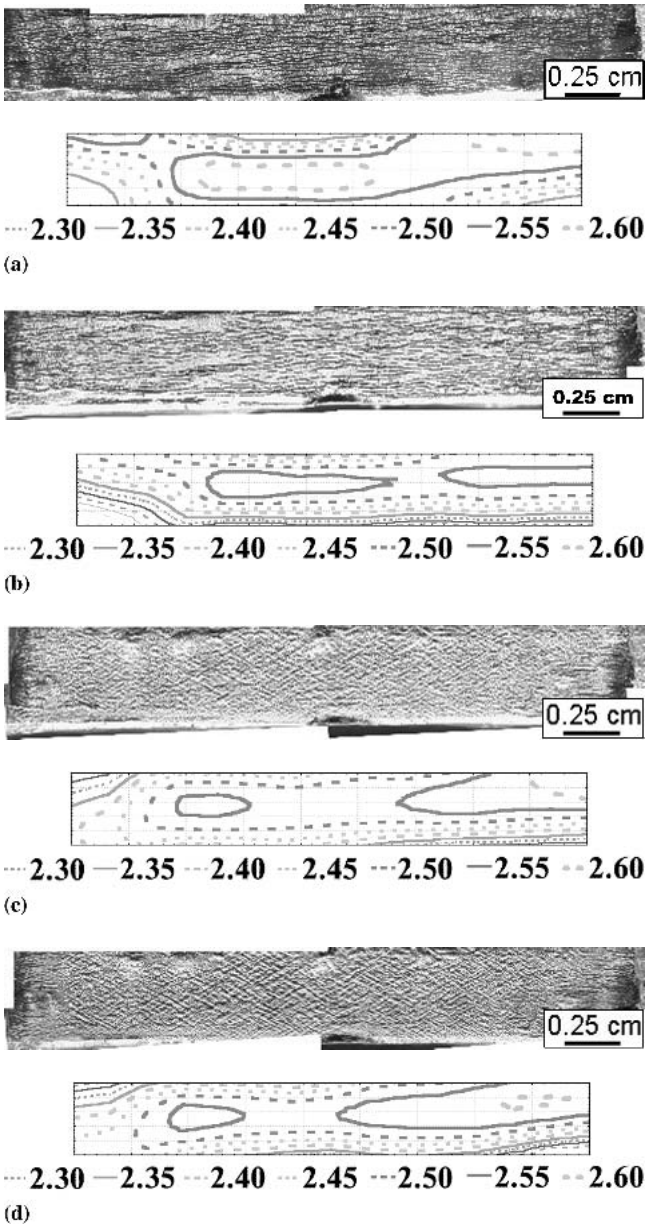

Fig. 11 Evolution of sensor surface (in several zones on flank side) visualized by panoramas and contour plots of information dimension: **(a)** 6000, **(b)** 12 000, **(c)** 200 000, and **(d)** 800 000 cycles

Evolution of a sensor surface visualized by panoramas and contour plots of information dimension are shown in Fig. 6. The very sharp rectangular contours clearly mark the shape of a sensor. The internal part of a sensor remains homogeneous, i.e., nearly the entire surface of a sensor can be characterized by a single value of information dimension.

The homogeneous character of surface relief in a parent metal gives a single value of information dimension *D*. As has been shown in our previous works,[4] the maximum of infor-

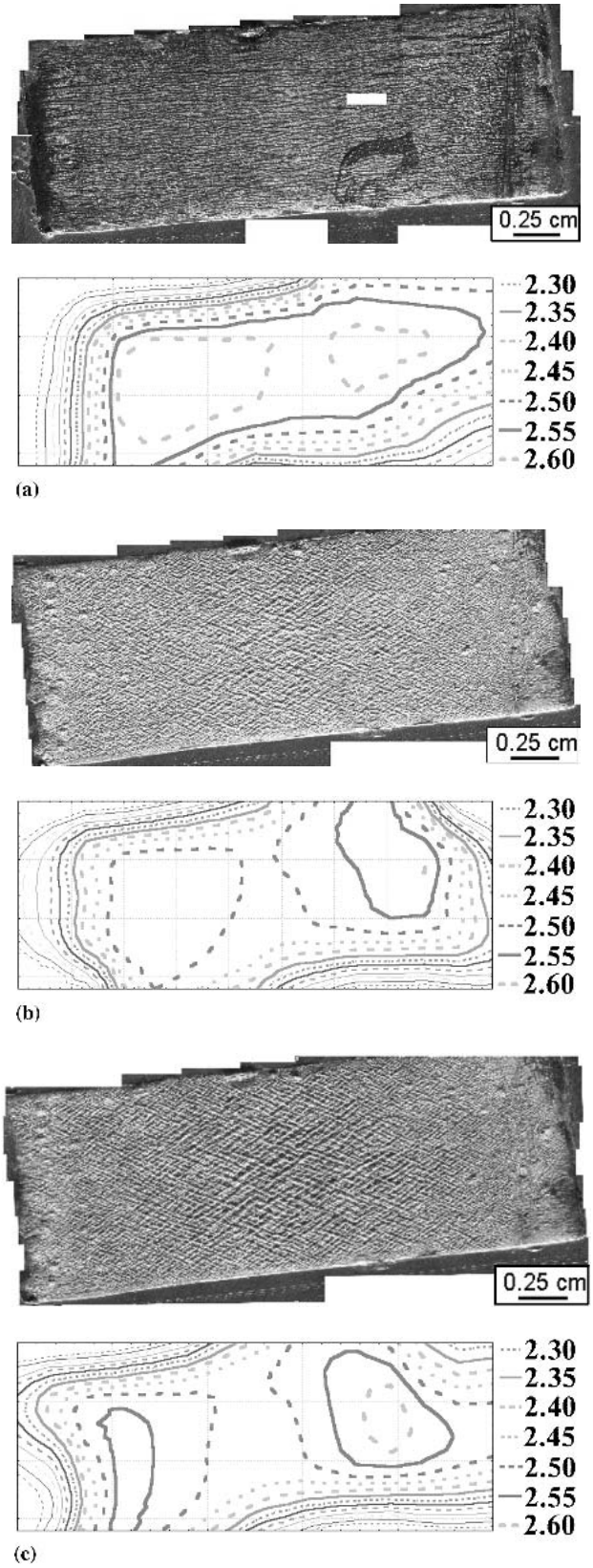

Fig. 12 Evolution of sensor surface (in several zones on narrow weld side) visualized by panoramas and contour plots of information dimension: **(a)** 6000, **(b)** 100 000, **(c)** 664000 cycles

mation dimension is characteristic of a critical state of material for higher numbers of cycles. In addition to this local peak, we observed the decrease of fractal dimension for the initial stage of loading. The high values of fractal dimension at this stage are probably caused by the appearance of the initial noisy patterns created by very small solitary intrusions and extrusions (<0.5 μm), which were observed by means of interference fringe patterns. Their further evolution leads to transformation of their random distribution to a uniform distribution in the very limited scale limits, with a decrease of the information fractal dimension.

3.3.2 TMAZ. This zone is situated directly after the parent metal with highest hardness and it is characterized by a slow decrease of hardness to the minimal value where a transition zone is located. The internal part of a sensor in this zone remains homogeneous, i.e., nearly the entire surface of a sensor can be characterized by a single value of information dimension, because its surface distribution has one pronounced peak with a very low standard deviation from the mean value. To some extent, it can be explained by proximity to the parent metal. Figure 7 shows typical panoramic views and fractal contour plots for panoramic views. The very sharp rectangular contours reflect the rectangular shape of a sensor.

3.3.3 Weld/TMAZ Transition Zone. This zone is very narrow and it has the minimal hardness value. In this connection, it could be the most probable place of strain localization and further fracture. In the range of high numbers of cycles, (before fracture of a specimen) the sensor relief becomes heterogeneous. In this connection, it could be the most probable place of strain localization and further fracture. However, panoramas and contour plots of information dimension significantly differ from those in the heat-affected zone only in the range of high numbers of cycles (before fracture of specimen). In this case, equidimensional plots change their uniform shape and become heterogeneous (Fig. 8). This can be the result of some crucial restructuring processes in an underlying specimen. Under these conditions, the relief description using a single value of the information dimension is of no value.

3.3.4 Weld. This zone is characterized by a neighborhood with two regions of the lowest hardness values: the two transition zones. For some numbers of cycles, an internal part of a sensor remains homogeneous, i.e., nearly the entire surface of a sensor can be characterized by a single value of the information dimension. The typical example of the information dimension evolution in a weld zone for stress level 201 MPa is shown in Fig. 9. The maximum of the information dimension can be observed for a high number of cycles. We again observed the pronounced decrease of fractal dimension at the initial stage of loading.

For the lowest stress level (≤175 MPa), however, nearly the entire surface of a sensor can be characterized by a single value of information dimension. Under these conditions, equidimensional plots have a uniform shape. For medium and highest stresses (Fig. 10), however, we observed some signs of strain localization in the shape of dumbbell discontinuities of a contour map in an intermediate stage, and increasing asymmetry of the equidimensional pattern for higher numbers of cycles. We suppose that it can be explained by some strain localization in some proximity of transition zones that cause such correlated restructuring in a sensor.

3.3.5 Flank Side. A sensor on the flank side covers several zones in a welded specimen. It is interesting to note that a weld and the transition zones have a trapezoidal cross section, and all differences of their internal structure and hardness can be visualized by equidimensional fractal maps (Fig. 11). Of course, the limited width of sensors in this zone (which is limited by the width of an underlying specimen) does not allow us to deduce some conclusions on heterogeneities along the shortest sides of sensors. Heterogeneous distribution of fractal dimension along the longest side, however, is quite obvious and coincides to some extent with the locations of the known soft zones.

3.3.6 Large Sensor on Narrow Weld Side. This zone is located in the central part of a specimen and a sensor covers several zones: a weld, weld/TMAZ transition zone, TMAZ, and parent metal. Figure 12 shows a relief of such a large sensor that is very heterogeneous, and a single value of the information dimension cannot describe such a structure. To provide a description, it is necessary to examine the distribution of the fractal dimension on the sensor area. From equidimensional maps, one can easily see two nearly symmetric heterogeneous regions with the maximal information dimension. They are located in places where transition zones are assumed to be. For the lowest stress value, these regions are not expressed in this manner, but they are more stable and pronounced for higher stresses.

4. Conclusions

In our work[4] we proposed to use a fractal analysis of single-crystal surface relief to estimate the deformation damage in complex aircraft alloys during fatigue loading. We carried out similar investigations with welded specimens of aircraft alloys with a priori known sites of stress concentration. These sites were revealed and investigated by a macrostructural optical method, x-ray methods, and hardness analysis.

We concluded that the qualitative topography analysis of a sensor surface remains a very efficient way to indirectly estimate the deformation history and deformation damage to monitor the number of cycles and stress amplitude of fatigue tests. Quantitative analysis, however, on the basis of calculations of information fractal dimension averaged by a sensor area does not apply for large sensors, which cover several zones with heterogeneous distribution of strains; for example, soft and hard zones near welds. Measuring the fractal dimension of a sensor surface and plotting the equidimensional maps allow us not only to find strain localization places, but also to envisage their dynamics. Note that large sensors, which can fully cover the possible area of stress localization, are necessary for this purpose. We used weld specimens only as examples of the structurally heterogeneous materials with a priori known zones with different structure and hardness.

Acknowledgments

The authors would like to thank Prof. Ron McEwen and Mr. Rostyslav Ilyushenko (BAE SYSTEMS, United Kingdom) for providing welded joints for investigations, as well as for technical support and useful discussions. This work was fulfilled under the framework of the INTAS-AIRBUS-1999-1547 project.

References

1. E. Zasimchuk, A. Radchenko, and M. Karuskevich: "Single Crystal Sensors of Fatigue Damage," *Fatigue Fract. Eng. Mater. Struct.*, 1992, *15*(12), pp. 1281-83.
2. Yu. Gordienko and E. Zasimchuk: "Single Crystal Indicators of Fatigue and Plastic Deformation Damage" in *Proceedings of Second European Conference on Smart Structures and Materials*, SPIE, Glasgow, Scotland, 1994, *2361*, pp. 312-15.
3. Yu. Gordienko, E. Zasimchuk, and M. Karuskevich: "Forecasting the Critical State of Deformed Crystal by Analysis of Smart Defect Structure: Fractal Characteristics and Percolation Critical Indexes" in *Proceedings of Seventh Conference on Sensors and Their Applications*, *Dublin, Ireland,* Institute of Physics Publishing, Bristol and Philadelphia, 1995, pp. 387-92.
4. E. Zasimchuk, Yu. Gordienko, M. Karuskevich, R. Gontareva, and I. Zasimchuk: "Technical Review as to Agreement Reference CJC/RMcE/081297 Between Institute of Metal Physics and Sowerby Research Centre," Internal Report, British Aerospace Systems (BAE), 1998.
5. I. Zasimchuk, E. Jivolub, and E. Pavlova: "Crystallographic Distortions Near Surface After Cutting Metal Single Crystals by Electrical and Chemical Methods," *Poverkhnost*, 1984, *9*, p. 142 (in Russian).
6. Yu.G. Gordienko, E.E. Zasimchuk, R. Gontareva, and V. Alexandrov: "Extra Dimensions by GIF-Animation: Industrial Opportunities for Online Monitoring Fatigue Tests of Metals in Intranet and the Web," *Int. J. Eng. Simul.*, 2000, *1*(3), pp. 2-8 (http://www.wlv.ac.uk/sebe/ijes/vol1num3/welcome.html).
7. B.B. Mandelbrot: *The Fractal Geometry of Nature*, Freeman, San Francisco, 1982, pp. 75–79.
8. F.C. Moon, *Chaotic Vibrations*, Wiley, New York, 1987, pp. 123–139.
9. Anon.: *Aluminum Alloys. Metal Science of Aluminum and Its Alloys*, Metallurgiya, Moscow, 1971 (in Russian).
10. H. Lipson and H. Steeple: *Interpretation of X-Ray Powder Diffraction Patterns*, St. Martin's Press, New York, 1970.
11. Yu.G. Gordienko, E.E. Zasimchuk, and M.V. Karuskevich: "Smart Sensors for Monitoring of Fatigue Damage and Exhaustion of Exploitation Resource in Intelligent Transportation System" in *Proceedings of the Automotive Transportation Technology Conference & Exposition 2001*, No. 2001-01-3178, Barcelona, Spain, 2001.